Dalton Transactions

ROYAL SOCIETY OF CHEMISTRY

PAPER

View Article Online
View Journal | View Issue

Open Access Article. Published on 25 February 2025. Downloaded on 5/20/2026 6:02:11 PM.
This article is licensed under a Creative Commons Attribution-NonCommercial 3.0 Unported Licence.

Check for updates

Cite this: *Dalton Trans.*, 2025, **54**, 5944

A novel type of heteroleptic Cu(I) complexes featuring nitrogen-rich tetrazine ligands: syntheses, crystal structures, spectral properties, cyclic voltammetry, and theoretical calculations†

Adam Sztula,[a] Peter Antal,[a] Ivan Nemec,[a] Martin Kubala[b] and Radovan Herchel*[a]

Heteroleptic copper(I) complexes with the general formula [Cu(N^N)(P^P)]X constitute one of the most studied categories of 3d metal photosensitizers. Here, we examine using 1,2,4,5-tetrazine-based ligands to synthesize photoactive Cu(I) complexes. The newly prepared complexes were characterized by single-crystal X-ray analysis, which revealed the formation of dinuclear complexes $[Cu_2(\mu\text{-}\mathbf{L1})(xantphos)_2](ClO_4)_2$ (**1**) and $[Cu_2(\mu\text{-}\mathbf{L2})(xantphos)_2](ClO_4)_2$ (**2**), and mononuclear complexes $[Cu(\mathbf{L3})(xantphos)]ClO_4$ (**3**) and $[Cu(\mathbf{L4})(xantphos)]ClO_4$ (**4**), where **L1** = 3,6-di(2′-pyridyl)-1,2,4,5-tetrazine (bptz), **L2** = 3,6-bis-(3,5-dimethyl-pyrazol-1-yl)-1,2,4,5-tetrazine, **L3** = 3-(2-pyridyl)-1,2,4,5-tetrazine, **L4** = 3-(3,5-dimethyl-1*H*-pyrazol-1-yl)-1,2,4,5-tetrazine and xantphos = 4,5-bis(diphenylphosphino)-9,9-dimethylxanthene. Solution stability assays were addressed by NMR spectroscopy showing that complexes are stable in dichloromethane over several days. The electronic excited states were investigated by UV-Vis and luminiscence spectroscopy and interpreted with the help of TD-DFT calculations. In the case of all the newly prepared complexes **1–4**, the absorptions in the visible region were assigned to non-emissive MLCT transitions between the Cu(I) and the respective tetrazine ligand. Redox properties were probed by cyclic voltammetry and also supplemented by DFT calculations. Interestingly, tetrazine ligands **L1–L4** show a shift of reduction potential to less negative values upon the formation of Cu(I) complexes **1–4**. Moreover, the two complexes **3–4** represent the first reported case of mononuclear heteroleptic Cu(I)–tetrazine complexes.

Received 8th November 2024,
Accepted 17th February 2025

DOI: 10.1039/d4dt03137g

rsc.li/dalton

Introduction

The fascinating nitrogen-based aromatic heterocycle 1,2,4,5-tetrazine, otherwise known as s-tetrazine (tz),[1] has entered the scope of coordination chemistry research only recently. A tetrazine ligand moiety is characterized by its electron-accepting capabilities, which stem from the four sp^2 nitrogen atoms bound in the same ring. The emergent low energy π* orbital of tz then allows for the formation of stable anionic radicals as well as enhanced reactivity, *e.g.*, in reverse electron demand Diels–Alder cycloadditions.[2] Ever since the s-tetrazine synthesis by Pinner,[3] and a reactive precursor 3,6-dichloro-tz were developed,[4] the road has been paved for the preparation of diverse tz-based complexes, summarized in a review by Kaim.[5] Discrete mono- or dinuclear complexes of tz derivatives are relatively common, however, the bulk of the work, that has been done so far, comprises mostly polymeric and polynuclear complexes or even MOFs (metal–organic framework) with the focus on their structural,[6] redox,[7] magnetic[8,9] or high energetic properties.[10,11]

Heteroleptic copper(I) complexes [Cu(N^N)(P^P)]X represent perhaps one of the largest groups of 3d metal complex photosensitizers. The mechanism of their photoactivity is nowadays well understood,[12,13] and the ongoing research is based on fine-tuning their applicability in various photonic schemes (*e.g.* in artificial photosynthesis,[14,15] photocatalysis,[16,17] OLED[18,19] and LEC devices[20,21]). Bulky bis(phosphines) as xantphos or POP are routinely chosen to chelate the Cu(I) center due to their steric demands and large bite angles. Many variations may be found in the literature regarding the choice of the nitrogen ligand. Usually, 1,10-phenanthroline and 2,2′-bipyridine derivatives are implemented, however, other ligands with nitrogen donor atoms, *e.g.* pyrazoles,[22] dipyrrinates,[23] oxazoles[24] and others,[25–27] described in the literature,

[a]*Department of Inorganic Chemistry, Faculty of Science, Palacký University, 17. listopadu 12, 77146 Olomouc, Czech Republic. E-mail: radovan.herchel@upol.cz*
[b]*Department of Experimental Physics, Faculty of Science, Palacký University, 17. listopadu 12, 77146 Olomouc, Czech Republic*

† Electronic supplementary information (ESI) available. CCDC 2392957–2392960. For ESI and crystallographic data in CIF or other electronic format see DOI: https://doi.org/10.1039/d4dt03137g

 This journal is © The Royal Society of Chemistry 2025

Open Access Article. Published on 25 February 2025. Downloaded on 5/20/2026 6:02:11 PM.
This article is licensed under a Creative Commons Attribution-NonCommercial 3.0 Unported Licence.

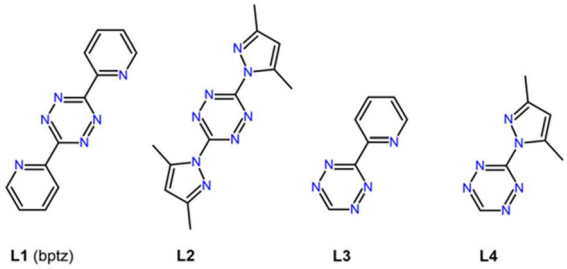

Fig. 1 Structures of ligands **L1–L4** used in this work.

have also been proven useful in terms of the resulting complex photoactivity. In this work, we evaluate tetrazine-based ligands (Fig. 1) for their inclusion in the viable nitrogen ligand pool for photoactive Cu(I) complexes.

A few luminescent Zn(II) and Cd(II) coordination polymers (without direct metal–tetrazine core bond) have been prepared based on 3,6-di(3′-pyridyl)-1,2,4,5-tetrazine and 3,6-di(4′-pyridyl)-1,2,4,5-tetrazine.[28] In these compounds, the innate tetrazine ligand emission (LLCT) is enhanced and blue-shifted by these metal centers, in other cases, the coordination of Zn(II) and Cd(II) ions have been shown to switch-on the luminescence of the tetrazine moiety.[29] Luminescent coordination polymers based on Cu(I/II) with tz ligands have been synthesized[30] as well as MOFs containing various M/S/Cu (M = W, Mo).[31] In Ru(II) complexes that do contain a direct metal–tetrazine bond, expected MLCT emission may be observed.[32,33]

Up to this day, only a handful of discrete heteroleptic Cu(I)–tetrazine complexes with a direct tz–Cu bond have been described with three general modes of bonding of the tz moiety: (a) radical anion bridging ligand,[34,35] (b) reduced form of H_2tz[36,37] or (c) basic form of tz heterocycle.[38,39] Most of the studies focus mainly on the structural and bonding properties of the resulting complexes with no emphasis on photophysical characterization.

Furthermore, the variety of stable oxidation forms of tz sparked our interest since Cu(I) photosensitizers undergo a brief charge separation process during the excitation event. We set out to investigate the structure and electronic properties of four novel heteroleptic Cu(I) complexes with xantphos and tetrazine ligands **L1–L4**.

Results and discussion

Synthesis and general characterization

Complexes **1–4** (Fig. 2) were synthesized using a standard procedure for the preparation of heteroleptic Cu(I) complexes. First, the diphosphine xantphos and $[Cu(ACN)_4]ClO_4$ were combined in dichloromethane, then the tetrazine ligand was added. Diffusion of an antisolvent into the solution resulted in the formation of crystals of the respective complexes. The newly prepared complexes were air-stable at room temperature and stable in dichloromethane (DCM) or chloroform solution,

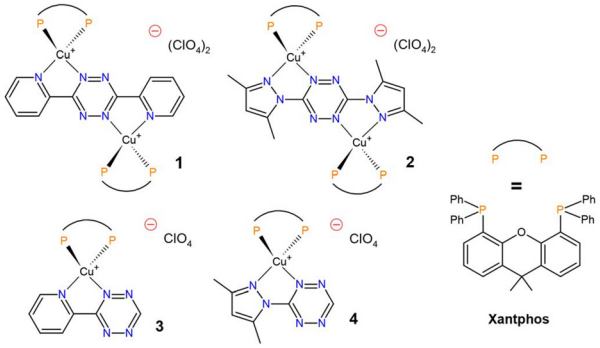

Fig. 2 Simplified scheme of complexes **1–4**.

with **1** and **2** being soluble only in the former. All the corresponding ^1H and $^{13}C\{^1H\}$ NMR signals of coordinated tetrazine and xantphos ligands were detected in the spectra of complexes in DCM. The stability of complexes **1–4** in DCM was confirmed, as no significant changes were detected in ^1H NMR spectra over 10 days (Fig. S1–S4†). Upon dissolution in coordinating solvents (acetonitrile, DMSO, methanol) the complexes decompose.

Crystal structures

X-ray quality single crystals of **1–4** were grown by slow diffusion of diethylether into dichloromethane solutions of the complexes. Compound **1** crystallizes in the monoclinic $P2_1/c$ space group, whereas compounds **2–4** crystallize in the monoclinic $P2_1/n$ space group. Selected crystallographic parameters for the compounds are summarized in Table S1.† The molecular structures of prepared complexes are shown in Fig. 3. The copper atoms in each of the complexes are four-coordinated by two phosphorus atoms from xantphos and two nitrogen atoms from tetrazine ligands. The shape of the coordination polyhedron was evaluated using SHAPE software

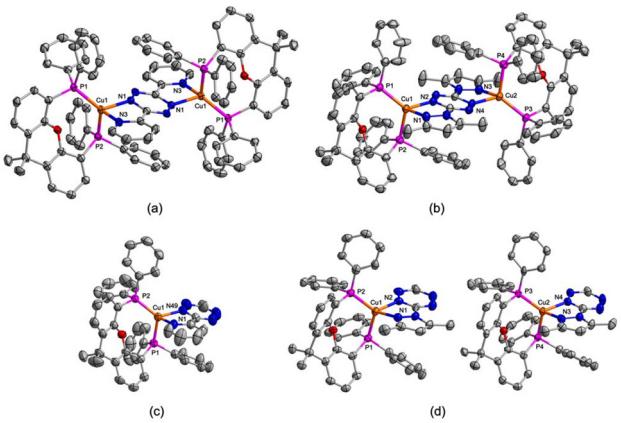

Fig. 3 Thermal ellipsoid plot with partial atom labelling depicting the complex cations in the crystal structure **1** (a), **2** (b), **3** (c), and **4** (d). The thermal ellipsoids are drawn at a 50% probability level. Hydrogen atoms and counterions are omitted for clarity.

Open Access Article. Published on 25 February 2025. Downloaded on 5/20/2026 6:02:11 PM.
This article is licensed under a Creative Commons Attribution-NonCommercial 3.0 Unported Licence.

(Table S2†), and the obtained continuous shape measures (CShM) indicate that the closest match is an axially vacant trigonal bipyramid (SHAPE's label vTBPY-4) for **1** and a tetrahedron (SHAPE's label T-4) for **2** and **3**. The asymmetric unit of **4** contains two slightly different copper coordination polyhedrons (Fig. 3, Tables S2 and S3†); one of them adopts the shape of an axially vacant trigonal bipyramid (Cu1), and the second (Cu2) is a tetrahedron, however, the obtained CShM values are very similar. The Cu–P and Cu–N bond distances in the compounds lie in ranges 2.21–2.30 and 2.02–2.09 Å, respectively. The values of the chelate angles N–Cu–N and P–Cu–P are very similar for each member of the series, with a much wider angle formed for the Xantphos (≈119°) than the heterocyclic ligand (≈79°). The values of the P–Cu–P and N–Cu–N angles, the angles between the PCuP and NCuN planes, and the N–C–C(N)–N torsion angles of N^N ligands (**L1–L4**) in crystal structures of **1–4** are similar with values observed for analogous structurally characterized $[Cu(xantphos)(N^N)]^+$ complexes, when N^N is 6- or 5-membered bicyclic aromatic ligand (Table S3†).

The crystal structure is stabilized by different types of non-covalent interactions. The complex cations of **1–3** exhibit π-stacking interactions between phenyl rings of xantphos and tetrazine ring (Fig. S5†). Numerous structurally characterized $[Cu(xantphos)(N^N)]^+$ complexes exhibit this interaction.[40–42] In compound **1**, the centroid···centroid distance is 3.54 Å, the centroid···plane distance is 3.42 Å, and the angle between the planes of the π-stacked rings is 10.8°. These parameters are 3.6 and 3.58 Å, 3.55 and 3.47 Å, 12.0 and 10.0° for **2** and 3.73 Å, 6.64 Å and 14.7° for **3**.

Spectral properties

UV-Vis spectra of ligands **L1–L4** and complexes **1–4** were measured in DCM – Fig. 4. The **L1** and **L2** ligands have strong absorption located at 33 800–34 000 cm^{-1}, while for **L3** and **L4**, it is shifted to higher energies at 36 500 cm^{-1} and 37 300 cm^{-1}, respectively. All ligands also show a weak absorption band at ~18 500 cm^{-1}. For dinuclear complexes **1** and **2**, we can see a shift of strong absorption bands to higher energies, 36 400 cm^{-1} and 37 200 cm^{-1}, respectively, while for mononuclear complexes **3** and **4**, the shift is minimal. The weak absorption band is almost unchanged for **1**, significantly shifted to lower energy for **2** to 13 700 cm^{-1}, slightly shifted to higher energy for **3** to 19 500 cm^{-1} and changed to 17 500 cm^{-1} for **4**.

With the aim to interpret data more deeply, the molecular and electronic structure of the ligands **L1–L4** and complexes $[Cu_2(\mu\text{-}\mathbf{L1})(xantphos)_2]^{2+}$ of **1**, $[Cu_2(\mu\text{-}\mathbf{L2})(xantphos)_2]^{2+}$ of **2**, $[Cu(\mathbf{L3})(xantphos)]^+$ of **3** and $[Cu(\mathbf{L4})(xantphos)]^+$ of **4** were theoretically studied at the DFT/TD-DFT level of theory using ORCA 5.0 software. The molecular structures were optimized with BP86 functional upon application of the C-PCM solvation model for dichloromethane, and the vibrational analyses confirmed the absence of imaginary frequencies. Thus, the proper convergence corresponding to the energy minimum was achieved (ESI, XYZ coordinates). Next, hybrid B3LYP functional

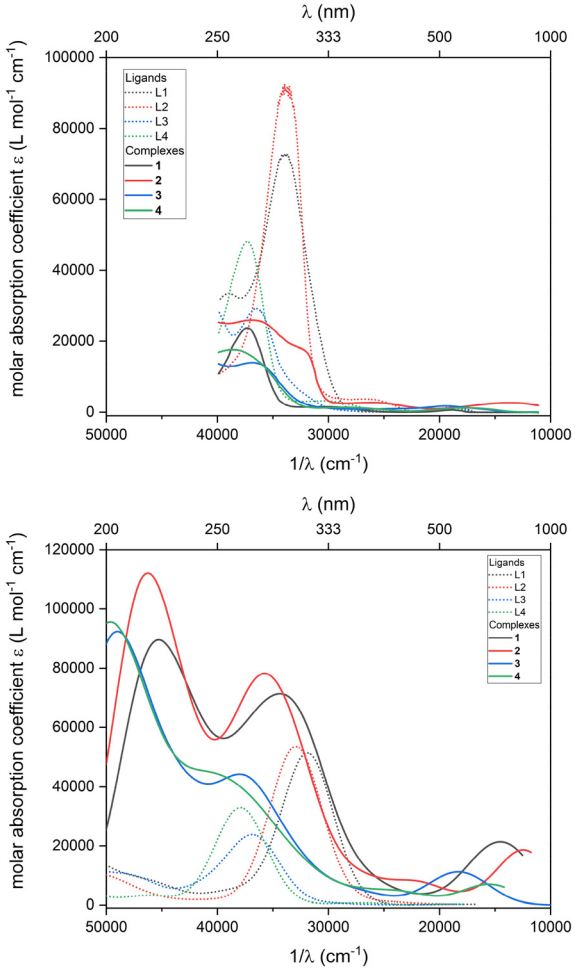

Fig. 4 The experimental (top) and TD-DFT calculated electronic spectra (bottom) for **L1–L4** and **1–4**.

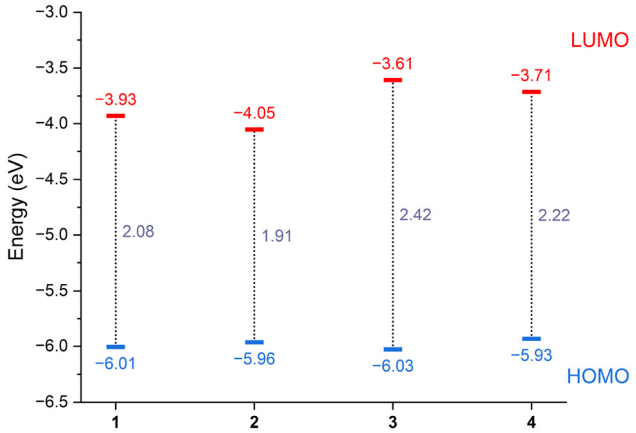

Fig. 5 Energy diagram showing the energies calculated of the HOMO, LUMO, and respective energy gaps of complexes **1–4**. The HOMO and LUMO are depicted in Fig. S6.†

was applied to calculate HOMO and LUMO and the respective energy gaps as shown in Fig. 5. The respective orbitals are depicted in Fig. S6.† It is evident that HOMOs are based on

 This journal is © The Royal Society of Chemistry 2025

Open Access Article. Published on 25 February 2025. Downloaded on 5/20/2026 6:02:11 PM.
This article is licensed under a Creative Commons Attribution-NonCommercial 3.0 Unported Licence.

copper and phosphorous atoms, whereas LUMOs are located on the tetrazine ring of the respective ligands **L1–L4**. Also, it seems that pyrazolyl-based ligands **L2** and **L4** provide smaller LUMO–HOMO energy gaps than pyridyl-based ligands **L1** and **L3**, which means that pyrazolyl groups act as more electron-withdrawing groups. The complexes can be ordered according to the increasing HOMO–LUMO gap as **2** < **1** < **4** < **3** with energy gaps varying from 1.91 to 2.42 eV (15 400 to 19 500 cm^{-1}).

In the next step, TD-DFT calculations were performed with B3LYP hybrid functional to compute the excited states and predict the absorption spectra for all compounds. Herein, the intensities calculated from the TD-DFT oscillator strengths were transformed into the molar absorption coefficients as implemented in Multiwfn. Generally, there is good agreement between the experimental and theoretical UV-VIS spectra, as shown in Fig. 4, and separately for ligands and complexes in Fig. S7 and S8.† Moreover, the analysis of the interfragment charge transfer during electron excitation (IFCT)[43] enabled us to analyze the individual contribution of the metal-centered states (MC), intra-ligand states (IL), metal-to-ligand charge transfer states (MLCT), ligand to-metal charge transfer states (LMCT), and ligand-to-ligand charge transfer states (LLCT) as shown in Fig. S13–S16.†

The first $S_0 \rightarrow S_1$ weak transition close to 20 000 cm^{-1} is located on tetrazine moiety ($n \rightarrow \pi^*$) for all **L1–L4** as also documented with natural transition orbitals (NTOs), while the strongest absorption around 32 000–38 000 cm^{-1} corresponds mainly to charge transfer from pyridine or pyrazole moiety to tetrazine moiety (Fig. S9–S12†).

In the case of **1**, the strong absorption band at ~34 300 cm^{-1} is formed dominantly by IL (**L1**), IL (xantphos), MLCT (Cu → **L1**), and LLCT (xantphos → **L1**) contributions. The weak absorption band at ~14 500 cm^{-1} is due to the prevailing contributions of LLCT (xantphos → **L1**) and MLCT (Cu → **L1**) – Fig. S13.†

For complex **2**, the strong absorption band at ~35 600 cm^{-1} is formed dominantly by IL (xantphos), LLCT (xantphos → **L2**) and LLCT between xantphos ligands. The weak absorption band at ~12 500 cm^{-1} is formed by the prevailing contributions of LLCT (xantphos → **L2**) and MLCT (Cu → **L2**). There is also another weaker band at ~22 000 cm^{-1} based on LLCT (xantphos → **L2**) – Fig. S14.†

In the case of **3**, the strong absorption band at ~37 800 cm^{-1} is based on prevailing IL (xantphos), IL (**L3**), MLCT (Cu → xantphos), and LLCT (**L3** → xantphos) contributions, while the weak absorption band at ~18 500 cm^{-1} is formed dominantly from LLCT (xantphos → **L3**), MLCT (Cu → **L3**) and IL (**L3**) contributions – Fig. S15.†

In the last complex **4**, the strong absorption band at ~39 000 cm^{-1} is dominated by IL (xantphos), LLCT (xantphos → **L4**), MLCT (Cu → xantphos) contributions. The weak absorption band at 15 500 cm^{-1} is formed mainly by LLCT (xantphos → **L4**) and MLCT (Cu → **L4**) and IL (**L4**) contributions – Fig. S16.†

To summarize, the MLCT between copper and tetrazine ligands **L1–L4** together with LLCT between xantphos and tetrazine ligands **L1–L4** are dominating contributions to absorption bands located at *ca.* 12 000–19 000 cm^{-1} in **1–4**, while ILCT and LLCT including xantphos and tetrazine ligands **L1–L4** significantly contribute to strong absorption bands above *ca.* 30 000 cm^{-1}.

Luminescence properties

Emissive properties of prepared complexes **1–4** were explored in degassed dichloromethane solutions (Fig. 6, Fig. S25†), solid phase (Fig. S26†), and KBr tablets (Fig. S27†). Several excitation wavelengths were chosen for each complex based on the respective absorption spectra (in nanometres): **1** and **2** (250, 300, 400, 550, 750), **3** (300, 400, 550, 600) and **4** (300, 350, 550, 600). Using the Agilent Cary Eclipse fluorescence spectrometer the emission was recorded up to 1100 nm. Usually, photosensitizers of the [Cu(N^N)(P^P)]X type with N^N ligands comprising phenanthroline and bipyridine derivatives exhibit MLCT band at ~400 nm with the resulting emission centred around 600 nm, however for complexes **1–4** no significant emission has been found (Fig. 6). In order to probe the emission properties in greater detail, some of the measurements were also taken on Horiba Fluorolog-3 fluorometer with high spectral resolution (Fig. S28†). Here, indeed, a faint emission may be observed for all complexes **1–4** at ~380 nm (ex. at 300 nm), which can be most likely attributed to the de-excitations from higher excited states.

To explain the low efficiency of the luminescence in herein studied complexes **1–4**, the additional DFT/TD-DFT calculations were performed in which also the archetype of [Cu(N^N)(P^P)]X class was involved, namely, the complex of Cu(I) with 2,9-dimethyl-1,10-phenanthroline (dmp): $[Cu(dmp)(xantphos)]^+$, for which is well-known good luminescence efficiency. First, the HOMO–LUMO gap of [Cu(dmp)

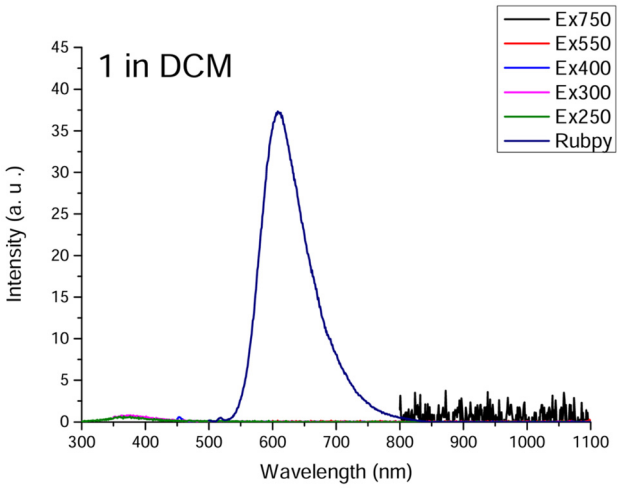

Fig. 6 Emission spectrum of complex **1** in degassed dichloromethane. Air equilibrated acetonitrile solution of $[Ru(bpy)_3](PF_6)_2$ (Rubpy) (with quantum yield of 0.018)[44] was also measured (ex. at 450 nm) to illustrate the instrument parameters. For all measured samples $A \approx 0.1$ at the excitation ($c \approx 3 \times 10^{-5}$–$5 \times 10^{-7}$ M).

Open Access Article. Published on 25 February 2025. Downloaded on 5/20/2026 6:02:11 PM.
This article is licensed under a Creative Commons Attribution-NonCommercial 3.0 Unported Licence.

(xantphos)]$^+$ was evaluated (Fig. S24†) to be 3.48 eV, and this value is much larger than the energy gap in complexes **1–4** (1.91 to 2.42 eV). Next, TD-DFT calculations provided vertical energies of the lowest excited singlets (S_1) and triplets (T_1), and again, [Cu(dmp)(xantphos)]$^+$ complex possesses larger energies than complexes **1–4** (Table 1). We also optimized the molecular geometries with multiplicity equal to three to obtain adiabatic energies of excited triplet states crucial to phosphorescence, and the energy of T_1 state for [Cu(dmp)(xantphos)]$^+$ is more than twice as large than energies of T_1 states in complexes **1–4** (Table 1).

Thus, we can rationalize the low luminescence efficiency of complexes **1–4** with the energy gap law,[45] which states that the rate of nonradiative decay increases exponentially as the energy gap between the excited state and the ground state decreases. This means that complexes **1–4** with smaller energy gaps than [Cu(dmp)(xantphos)]$^+$ are more likely to lose energy through nonradiative processes rather than through luminescence.

Redox properties

Cyclic voltammetry measurements for ligands **L1–L4** and complexes **1–4** are presented in Fig. S17–S21,† Fig. 7 and Table S6.† The tz ligands are known for their accessibility to acquiring electrons and being reduced, and based on the different substituents, their reduction potential varies between −1.7 and −0.9 V *vs.* Fc$^+$/Fc.[1] Indeed, herein ligands **L1** and **L3** bearing pyridinyl-substituents have more negative reduction potential in comparison to pyrazolyl-substituted tetrazines **L2** and **L4**. Overall, the trend for $E_{1/2(n/red)}$ is as follows **L1** (−1.34) < **L3** (−1.32) < **L4** (−1.17) < **L2** (−1.05) < 0 *vs.* Fc$^+$/Fc. Furthermore, DFT methods were applied to study the redox properties of presented ligands **L1–L4**, whereas the same procedure as from TD-DFT calculations was applied; concretely, the molecular geometries were optimized with BP86 functional, and single-point energies were calculated with B3LYP functional. Again, the C-PCM solvation model for dichloromethane was used. Next, the standard Gibbs free energies of these redox half-reactions

$$^1[Lx] + e^- \rightarrow {}^2[Lx]^- \qquad E_{n/red}\ (x = 1\text{–}4)$$

were obtained and transformed to standard redox potentials with the help of $\Delta_r G_{ox/red} = -zFE_{ox/red}$ relationship. Finally, these absolute redox potentials were compared to the ferrocenium/ferrocene (Fc$^+$/Fc) couple and are reported in Table 2. The calculated $E_{n/red}$ for **L1–L4** are in the range from −0.9 to −1.2 V, with **L1** and **L3** having the most negative potential, which agrees with the experimental measurements. The calculated spin densities of reduced **L1–L4** ligands show the formation of tetrazine radicals (Fig. S22†). We also theoretically inspected successive reductions to dianion species as

$$^2[Lx]^- + e^- \rightarrow {}^1[Lx]^{2-} \qquad E_{red/red2}\ (x = 1\text{–}4)$$

However, these reduction potentials adopted values from −3.3 to −2.9 V *vs.* Fc$^+$/Fc (Table 2), which is outside the experimental range.

Next, measurements on copper complexes **1–4** revealed quasireversible redox processes in the range from −0.82 to −0.24 V *vs.* Fc$^+$/Fc, which were attributed to the reduction of the respective tetrazine ligands and formation of the complexes with radical tetrazine moiety. Shift to less negative values of reduction potential in copper complexes in comparison to free ligands can be explained by the formation of sigma-coordination bonds, and as tetrazine ligands act as Lewis bases, these coordinated ligands can more easily accommodate extra electron. Indeed, the dinuclear species **1** (−0.38 V) and **2**

Table 1 DFT/TD-DFT energies (eV) of excited singlet and triplet for **1–4** and [Cu(dmp)(xantphos)]$^+$

	$\varepsilon(S_1)$–$\varepsilon(S_0)^a$	$\varepsilon(T_1)$–$\varepsilon(S_0)^a$	$\varepsilon(T_1)$–$\varepsilon(S_0)^b$
1	1.64	1.06	0.88
2	1.53	0.92	0.78
3	2.07	1.27	0.91
4	1.86	1.16	0.86
[Cu(dmp)(xantphos)]$^+$	2.86	2.58	2.28

[a] The vertical energies derived from TD-DFT calculations on optimized singlet molecular geometries. [b] The adiabatic energies derived from the comparison of energies resulting from optimized geometries of triplet and singlet multiplicities.

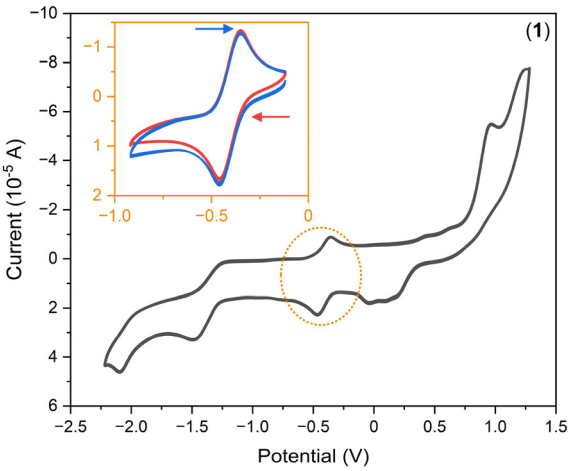

Fig. 7 Cyclic voltammogram of complex **1** *vs.* Fc$^+$/Fc.

Table 2 The redox potential *E* (V) *vs.* Fc$^+$/Fc couple computed by DFT methods

Compound	$E_{ox2/ox1}$ (V)	$E_{ox1/n}$ (V)	$E_{n/red}$ (V)	$E_{red/red2}$ (V)
1	1.755	1.182	−0.228	
2	1.625	1.214	−0.089	
3		1.074	−0.555	
4		1.028	−0.482	
L1			−1.181	−2.894
L2			−0.903	−2.927
L3			−1.153	−3.340
L4			−1.033	−3.175

 This journal is © The Royal Society of Chemistry 2025

Open Access Article. Published on 25 February 2025. Downloaded on 5/20/2026 6:02:11 PM.
This article is licensed under a Creative Commons Attribution-NonCommercial 3.0 Unported Licence.

(−0.29) have less negative reduction potential than mononuclear complexes **3** (−0.82 V) and **4** (−0.73 V) *vs.* Fc^+/Fc.

In cases **1** and **3**, the irreversible redox signal is observed at 0.96 and 0.98 V, respectively, which can be assigned to metal-centered oxidation to Cu(II) species. Moreover, the irreversible redox processes are observed at *ca.* −1.48 for **1–4**, which are difficult to assign, but very similar values suggest that the same decomposition product must be involved.

To support our interpretation of CV experiments for **1–4**, the DFT calculations of reduction potential were also calculated for several redox processes as outlined in these electrochemical reactions:

$$^{3}\left[Cu_2(\mu\text{-L}x)(\text{xantphos})_2\right]^{4+} + e^- \rightarrow {}^{2}\left[Cu_2(\mu\text{-L}x)(\text{xantphos})_2\right]^{3+} \quad E_{ox2/ox1}(x = 1-2)$$

$$^{2}\left[Cu_2(\mu\text{-L}x)(\text{xantphos})_2\right]^{3+} + e^- \rightarrow {}^{1}\left[Cu_2(\mu\text{-L}x)(\text{xantphos})_2\right]^{2+} \quad E_{ox1/n}(x = 1-2)$$

$$^{1}\left[Cu_2(\mu\text{-L}x)(\text{xantphos})_2\right]^{2+} + e^- \rightarrow {}^{2}\left[Cu_2(\mu\text{-L}x)(\text{xantphos})_2\right]^{+} \quad E_{n/red}(x = 1-2)$$

$$^{2}[Cu(Lx)(\text{xantphos})]^{2+} + e^- \rightarrow {}^{1}[Cu(Lx)(\text{xantphos})]^{+} \quad E_{ox1/n}(x = 3-4)$$

$$^{1}[Cu(Lx)(\text{xantphos})]^{+} + e^- \rightarrow {}^{2}[Cu(Lx)(\text{xantphos})]^{0} \quad E_{n/red}(x = 3-4)$$

and the data are summarized in Table 2. In the case of mononuclear complexes **3** and **4**, the calculated $E_{n/red}$ values are shifted to *ca.* −0.5 V, which means that the formation of tz-radical can be achieved more easily. The calculated spin densities of these complexes are shown in Fig. S23.† The metal-centered oxidation potentials $E_{ox1/n}$ of **3** and **4** have values close to 1.0 V, and these values are comparable to other [Cu(N^N)(P^P)]X complexes with bipyridyl derivatives.[46,47]

The calculated $E_{n/red}$ values for dinuclear complexes **1** and **2** are shifted to less negative values (−0.228 for **1** and −0.089 V for **2**), which implies that they are more prone to reduction than **3** and **4**. The metal-centered oxidation potentials $E_{ox1/n}$ of **1** (1.182 V) and **2** (1.214) are slightly higher than for mononuclear species, and the second oxidation would require $E_{ox2/ox1}$ around 1.6–1.7 V (Table 2). It must also be noted that Mulliken population analysis suggests that spin density on oxidized species is partially transferred to the xantphos ligand, most likely due to the π-acceptor properties of such a ligand.

Experimental

Materials and methods

Regular and deuterated solvents, as well as chemicals, were purchased from commercial sources (VWR International or Sigma-Aldrich) and used as received. Xantphos was purchased from Apollo Scientific. For column chromatography, Silica gel 60 (0.015–0.04 mm, Macherey-Nagel GmbH & Co. KG) was used. Ligands **L1–L4** were prepared according to respective literature procedures: **L1**,[48] **L3**,[49] **L2** and **L4**.[50] $[Cu(ACN)_4]ClO_4$ was prepared according to literature[51] and used without further purification or analysis.

^{1}H, ^{13}C{^{1}H} and ^{31}P{^{1}H} NMR spectra were recorded at room temperature in CD_2Cl_2 using a Varian 400 MHz spectrometer, ^{1}H and ^{13}C{^{1}H} chemical shifts were referenced to residual solvent peak ^{1}H (CD_2Cl_2) = 5.32 ppm and ^{13}C{^{1}H} (CD_2Cl_2) = 53.4 ppm. The ^{31}P{^{1}H} chemical shifts are referenced to δ(85% aq. H_3PO_4) = 0. Absorption spectra were measured on Cintra 3030 double-beam UV-Vis spectrometer in dichloromethane. Emission spectra were taken on Agilent Cary Eclipse fluorescence spectrometer (degassed dichloromethane solutions, solid phase and KBr tablets) at room temperature with scan rate 600 nm min^{-1}, 1 nm step and averaging time 0.1 s. Bandpasses were set to 5 nm in both the excitation and emission monochromator. Steady-state emission spectra of the **1–4** degassed solutions in dichloromethane were also recorded on Fluorolog-3 fluorometer (Jobin–Yvon, France) using excitation wavelength at 300 nm in the interval 320–570 nm with the 1 nm step and integration time 1 s per data point, bandpasses were set to 5 nm in both the excitation and emission monochromator. Spectra were recorded under room temperature, and the signal from pure solvent was subtracted as a background. Elemental analysis was performed using Thermo Scientific Flash 2000 analyzer. Infrared spectra were collected on Jasco FT/IR-4700 spectrometer using the ATR technique on a diamond plate in the range of 400–4000 cm^{-1}. Cyclic voltammetry was performed using CHI600C potentiostat with $[nBu_4N][ClO_4]$ (0.1 M) as a supporting electrolyte at a scan rate of 0.1 V s^{-1}. A standard three-electrode arrangement was employed using glassy carbon as a working electrode, platinum wire counter-electrode and Ag/AgCl reference electrode filled with the supporting electrolyte solution. The solutions of complexes and ligands (*ca.* 1 × 10^{-3} M) were deaerated with argon bubbling. The final potentials are referenced to the Fc/Fc^+ couple.

Synthesis of $[Cu_2(\mu\text{-L1})(\text{xantphos})_2](ClO_4)_2$ (1)

$[Cu(ACN)_4]ClO_4$ (65 mg, 0.20 mmol) was dissolved in 10 ml of dichloromethane and xantphos (116 mg, 0.20 mmol) was added. The solution was stirred at room temperature for 1 hour, then **L1** (24 mg, 0.10 mmol) was added all at once followed by immediate darkening of the solution. After further 2 hours of stirring at room temperature, the reaction mixture was filtered, and the solution was left to crystallize slowly by diffusion of diethylether. In a few days, dark-blue, X-ray quality crystals formed, they were then filtered off, washed with diethylether and dried on high vacuum at room temperature. Yield: 120 mg (70%). **^{1}H NMR** (CD_2Cl_2, 400 MHz, 25 °C): δ = 8.49 (t, 2H, J = 7.5, **L1**–H), 8.45–8.37 (m, 4H, **L1**–H), 7.87 (t, 2H, J = 6.0, **L1**–H), 7.76 (d, 4H, J = 8.0, Ar–H), 7.44 (t, 4H, J = 7.0, Ar–H), 7.36–7.19 (m, 20H, Ar–H), 7.07 (t, 4H, J = 7.5, Ar–H), 6.93 (t, 8H, J = 7.0, Ar–H), 6.74–6.60 (m, 12H, Ar–H), 1.92 (s, 6H, CH_3), 1.60 (s, 6H, CH_3). **^{13}C{^{1}H} NMR** (CD_2Cl_2, 25 °C): δ = 154.6, 150.1, 145.2, 140.6, 133.9, 133.0, 132.0, 131.4, 131.0,

Open Access Article. Published on 25 February 2025. Downloaded on 5/20/2026 6:02:11 PM. This article is licensed under a Creative Commons Attribution-NonCommercial 3.0 Unported Licence.

130.3, 129.2, 129.0, 125.6, 125.3, 36.0, 30.1, 28.3, 25.7. **$^{31}P\{^1H\}$ NMR** (CD_2Cl_2, 25 °C): δ = −9.5. **FTIR** (ATR, cm^{-1}): 3054(m), 2975(m), 1594(w), 1478(m), 1435(m), 1405(s), 1397(s), 1231(m), 1204(w), 1084(vs), 877(w), 741(s), 695(s), 621(m), 514(m), 500(m), 457(m). **Anal. calc.** for **1** ($C_{90}H_{72}Cl_2Cu_2N_6O_{10}P_4$·3/2$CH_2Cl_2$): C, 59.51; H, 4.09; N, 4.55. **Found**: C, 59.79; H, 3.93; N, 4.42.

Synthesis of [Cu_2(μ-L2)(xantphos)$_2$](ClO_4)$_2$ (2)

Complex **2** was prepared by following a similar procedure as for complex **1** using **L2** (27 mg, 0.10 mmol) instead of **L1**. Yield: 135 mg (77%) of dark-green crystals. **^1H NMR** (CD_2Cl_2, 400 MHz, 25 °C): δ = 7.69 (t, 4H, J = 8.0, Ar–H), 7.46–7.38 (m, 4H, Ar–H), 7.30–7.17 (m, 20H, Ar–H), 7.12 (t, 4H, J = 7.5, Ar–H), 7.04 (t, 8H, J = 7.5, Ar–H), 6.82–6.71 (m, 12H, Ar–H), 6.44 (s, 2H, **L2**–H), 2.54 (s, 6H, **L2**–CH_3), 1.87 (s, 6H, CH_3), 1.52 (s, 6H, **L2**–CH_3), 1.51 (s, 6H, CH_3). **$^{13}C\{^1H\}$ NMR** (CD_2Cl_2, 25 °C): δ = 154.5, 145.5, 133.7, 132.9, 132.4, 131.3, 130.7, 130.3, 129.1, 129.0, 129.0, 128.2, 125.3, 114.1, 35.9, 31.6, 25.1, 15.1, 14.8, 13.2. **$^{31}P\{^1H\}$ NMR** (CD_2Cl_2, 25 °C): δ = −11.1. **FTIR** (ATR, cm^{-1}): 3051(w), 2971(m), 1580(w), 1486(m), 1452(s), 1434(s), 1402(vs), 1233(sh), 1217(m), 1082(vs), 975(m), 872(w), 746(m), 693(m), 621(m), 515(m), 499(m), 462(w). **Anal. calc.** for **2** ($C_{90}H_{78}Cl_2Cu_2N_8O_{10}P_4$·2/3$CH_2Cl_2$): C, 60.16; H, 4.42; N, 6.19. **Found**: C, 60.07; H, 4.25; N, 6.00.

Synthesis of [Cu(L3)(xantphos)](ClO_4) (3)

Complex **3** was prepared by following a similar procedure as for complex **1**. Chloroform (10 ml) was used as the solvent rather than dichloromethane and **L3** (32 mg, 0.20 mmol) instead of **L1**. Yield: 86 mg (48%) of dark-purple crystals. **^1H NMR** (CD_2Cl_2, 400 MHz, 25 °C): δ = 10.33 (s, 1H, **L3**–H), 8.98 (d, 1H, J = 8.0, **L3**–H), 8.31 (t, 1H, J = 8.0, **L3**–H), 8.12 (d, 1H, J = 5.0, **L3**–H), 7.73 (d, 2H, J = 8.0, Ar–H), 7.70 (m, 1H, **L3**–H), 7.38–7.33 (m, 2H, Ar–H), 7.31–7.18 (m, 12H, Ar–H, 1H, $CHCl_3$), 7.10 (t, 4H, J = 7.5, Ar–H), 6.72–6.61 (m, 6H, Ar–H), 1.94 (s, 3H, CH_3), 1.56 (s, 3H, CH_3). **$^{13}C\{^1H\}$ NMR** (CD_2Cl_2, 25 °C): δ = 160.9, 159.4, 154.7, 154.6, 154.6, 149.6, 146.4, 139.9, 133.9, 132.8, 132.4, 131.4, 130.3, 130.1, 128.9, 128.1, 125.8, 125.1, 125.1, 118.3, 118.2, 118.0, 36.0, 31.2, 25.2. **$^{31}P\{^1H\}$ NMR** (CD_2Cl_2, 25 °C): δ = −10.7. **FTIR** (ATR, cm^{-1}): 3060(w), 2975(m), 1598(w), 1479(m), 1434(s), 1403(vs), 1346(m), 1238(m), 1084(vs), 879(w), 742(m), 694(m), 621(m), 514(m), 505(sh), 460(w). **Anal. calc.** for **3** ($C_{46}H_{37}ClCuN_5O_5P_2$·2/3$CHCl_3$): C, 57.17; H, 3.87; N, 7.14. **Found**: 57.07; H, 3.68; N, 6.77.

Synthesis of [Cu(L4)(xantphos)](ClO_4) (4)

Complex **4** was prepared by following a similar procedure as for complex **3**. **L4** (35 mg, 0.20 mmol) was used instead of **L3**. Yield: 183 mg (99%) of dark-red crystals. **^1H NMR** (CD_2Cl_2, 400 MHz, 25 °C): δ = 10.18 (s, 1H, **L4**–H), 7.69 (d, 2H, J = 8.0, Ar–H), 7.39–7.27 (m, 8H, Ar–H), 7.27–7.14 (m, 9H, Ar–H, 1.5H, $CHCl_3$), 6.80–6.73 (m, 4H, Ar–H), 6.73–6.67 (m, 2H, Ar–H), 6.45 (s, 1H, **L4**–CH_3), 2.83 (s, 3H, **L4**–CH_3), 1.92 (s, 3H, CH_3), 1.49 (s, 3H, CH_3), 1.46 (s, 3H, HC). **$^{13}C\{^1H\}$ NMR** (CD_2Cl_2, 25 °C): δ = 157.5, 155.5, 154.7, 146.5, 133.7, 133.0, 132.9, 132.5, 131.3, 130.3, 128.9, 128.0, 125.1, 114.1, 35.9, 32.1, 24.5, 15.1, 13.0. **$^{31}P\{^1H\}$ NMR** (CD_2Cl_2, 25 °C): δ = −12.3. **FTIR** (ATR, cm^{-1}): 3051(w), 2977(w), 1581(w), 1483(m), 1435(m), 1403(vs), 1226(m), 1083(vs), 937(w), 874(w), 741(m), 692(m), 621(m), 507(m), 466(w). **Anal. calc.** for **4** ($C_{46}H_{40}ClCuN_6O_5P_2$·3/2$CHCl_3$): C, 52.01; H, 3.81; N, 7.66. **Found**: C, 52.11; H, 3.62; N, 7.40.

Crystallography

Suitable single crystals of **1–4** were grown by slow diffusion of diethylether into dichloromethane (**1** and **2**) or chloroform (**3** and **4**) solutions of the complexes. Data collection for complexes was done using an XtaLAB Synergy-I diffractometer with a HyPix3000 hybrid pixel array detector and microfocused PhotonJet-I X-ray source (Cu Kα). The data integration, scaling, and absorption for correction were applied using the program CryAlisPro 1.171.40.82a.[52]

The structures were solved using SHELXT[53] program and refined by the full matrix least-squares procedure with SHELXL[54] in OLEX2[55] (version 1.3). All hydrogen atoms were found in differential Fourier maps, and their parameters were refined using a riding model with U_{iso}(H) = 1.2(CH, –CH_2) or 1.5(–CH_3)U_{eq}. Figures with detailed structure details were drawn using Diamond[56] software.

Non-routine aspects of refinement:

The perchlorate anions were disordered in crystal structures **2–4**, and in all cases, this was modelled as positional disorder over two positions.

Solvent masking[57] was applied to mask the electron density of disordered and superimposed solvent molecules in the following cases:

2 (masked electron density corresponds to 2.5 CH_2Cl_2 molecules per asymmetric unit),

3 (masked electron density corresponds to 0.5 $CHCl_3$ molecule per asymmetric unit),

4 (masked electron density corresponds to 1 $CHCl_3$ molecule per asymmetric unit).

The CIF files were deposited into the Cambridge Structural database under the following deposition numbers: 2392957–2392960.†

Theoretical calculations

The theoretical calculations were done with ORCA 5.0 quantum chemistry software.[58] The molecular geometries of the ligands **L1–L4** and complexes [Cu_2(μ-**L1**)(xantphos)$_2$]$^{2+}$ of **1**, [Cu_2(μ-**L2**)(xantphos)$_2$]$^{2+}$ of **2**, [Cu(**L3**)(xantphos)]$^+$ of **3** and [Cu(**L4**)(xantphos)]$^+$ of **4** were extracted from X-ray data and optimized with BP86 functional[59] together with the atom-pairwise dispersion correction (D4).[60] The def2-TZVP basis set was used for all atoms.[61] The calculations were speed-up using def2/J Coulomb fitting basis set[62] and RIJCOSX approximation.[63] The largest integration grid (DefGrid3) and tightSCF convergence criteria were used in all calculations. Also, the implicit solvation model C-PCM was used during geometry optimization.[64,65] The hybrid B3LYP+D4 functional was used

Open Access Article. Published on 25 February 2025. Downloaded on 5/20/2026 6:02:11 PM.
This article is licensed under a Creative Commons Attribution-NonCommercial 3.0 Unported Licence.

to calculate the final energies of the complexes,[66] HOMO and LUMO energies, and was also used for TD-DFT calculations. A similar approach was applied to $[Cu(dmp)(xantphos)]^+$. The calculated data were visualized with VESTA 3 program.[67]

Conclusions

To conclude, four new heteroleptic Cu(I) complexes have been prepared and characterized by X-ray analysis, cyclic voltammetry, NMR spectroscopy, UV-Vis, and luminescence spectroscopies, including DFT theoretical calculations. Newly prepared Cu(I) complexes are stable in solid form and in solutions of non-coordinating solvents. Unlike most of Cu(I) species of the [Cu(N^N)(P^P)]X type with N^N ligands comprising phenanthroline and bipyridine derivatives, complexes **1–4** show very low luminescence efficiency due to much lower energy gaps to first excited singlet and triplet states than complexes with phenanthroline-like ligands. This renders tetrazine-based ligands in the preparation of photoactive Cu(I) complexes unsuitable unless the introduction of other substituents and modification of the electronic structure of tetrazine would lead to a significant increase in HOMO–LUMO energy gap. Another possible strategy would be a modification of the tetrazine core by cycloaddition as was proven useful in different metal complexes.[68] Interesting reversible redox properties have been recorded for reported compounds, showing that upon complex formation, the reduction of coordinated tetrazine ligands **L1–L4** is becoming more accessible.

Author contributions

Adam Sztula: Investigation, writing – original draft Peter Antal: Conceptualization, methodology, visualization Ivan Nemec: Investigation, formal analysis Martin Kubala: Investigation, formal analysis Radovan Herchel: Conceptualization, software, formal analysis, writing – review & editing.

Data availability

The data supporting this article have been included as part of the ESI.†

Conflicts of interest

There are no conflicts to declare.

Acknowledgements

The authors thankfully acknowledge the financial support from Palacký University in Olomouc projects IGA_PrF_2023_007 and IGA_PrF_2024_009. The authors are grateful to P. Richterová for the elemental analysis measurements.

References

1 G. Clavier and P. Audebert, *Chem. Rev.*, 2010, **110**, 3299.
2 M. L. Blackman, M. Royzen and J. M. Fox, *J. Am. Chem. Soc.*, 2008, **130**, 13518.
3 A. Pinner, *Chem. Ber.*, 1893, **26**, 2126.
4 D. E. Chavez and M. A. Hiskey, *J. Energ. Mater.*, 1999, **17**, 357.
5 W. Kaim, *Coord. Chem. Rev.*, 2002, **230**, 127.
6 I. D. Giles, H. T. Chifotides, M. Shatruk and K. A. Dunbar, *Chem. Commun.*, 2011, **47**, 12604.
7 C. R. Benson, A. K. Hui, K. Parimal, B. J. Cook, C. H. Chen, R. L. Lord, A. H. Flood and K. G. Caulton, *Dalton Trans.*, 2014, **43**, 6513.
8 M. A. Lemes, N. Mavragani, P. Richardson, Y. Zhang, B. Gabidullin, J. L. Brusso, J. O. Moilanen and M. Murugesu, *Inrog. Chem. Front.*, 2020, **7**, 2592.
9 B. S. Dolinar, S. Gómez-Coca, D. I. Alexaxandropoulos and K. R. Dunbar, *Chem. Commun.*, 2018, **53**, 2283.
10 T. W. Myers, J. A. Bjorgaard, K. E. Brown, D. E. Chavez, S. K. Hanson, R. J. Scharff, S. Tretiak and J. M. Veauthier, *J. Am. Chem. Soc.*, 2016, **138**, 4685.
11 T. W. Myers, D. E. Chavez, S. K. Hanson, R. J. Scharff, B. L. Scott, J. M. Veauthier and R. Wu, *Inorg. Chem.*, 2015, **54**, 8077.
12 M. S. Lazorski and F. N. Castellano, *Polyhedron*, 2014, **82**, 57.
13 Y. Zhang, M. Schulz, M. Wächtler, M. Karnahl and B. Dietzek, *Coord. Chem. Rev.*, 2018, **356**, 127.
14 S. P. Luo, E. Mejía, A. Friedrich, A. Pazidis, H. Junge, A. E. Surkus, R. Jackstell, S. Denurra, S. Gladiali, S. Lochbrunner and M. Beller, *Angew. Chem., Int. Ed.*, 2013, **52**, 419.
15 L. X. Xu, T. Q. Wang, X. F. Liu, H. Chen, C. J. Wei, D. D. Xu, F. Chen, Y. Li and S. P. Luo, *Eur. J. Inorg. Chem.*, 2020, **2020**, 4278.
16 H. Takeda, Y. Monma, H. Sugiyama, H. Uekusa and O. Ishitani, *Front. Chem.*, 2019, **7**, 418.
17 S. Paria and O. Reiser, *ChemCatChem*, 2014, **6**, 2477.
18 R. C. Evans, P. Douglas and C. J. Winscom, *Coord. Chem. Rev.*, 2006, **250**, 2093.
19 D. Liang, X. L. Chen, J. Z. Liao, J. Y. Hu, J. H. Jia and C. Z. Lu, *Inorg. Chem.*, 2016, **55**, 7467.
20 C. E. Housecroft and E. C. Constable, *J. Mater. Chem. C*, 2022, **10**, 4456.
21 R. D. Costa, D. Toreda, E. Ortí, H. J. Bolink, J. Schönle, S. Graber, C. E. Housecroft, E. C. Constable and J. A. Zampese, *J. Mater. Chem.*, 2011, **11**, 16108.
22 G. Farias, C. A. M. Salla, J. Toigo, L. G. T. A. Duarte, A. J. Bortoluzzi, E. Girotto, H. Gallardo, T. B. Z. Atvars, B. de Souza and I. H. Bechtold, *Dalton Trans.*, 2022, **51**, 1008.
23 X. Liu, H. Nan, W. Sun, Q. Zhang, M. Zhan, L. Zou, Z. Xie, X. Li, C. Lu and Y. Cheng, *Dalton Trans.*, 2012, **41**, 10199.

Open Access Article. Published on 25 February 2025. Downloaded on 5/20/2026 6:02:11 PM.
This article is licensed under a Creative Commons Attribution-NonCommercial 3.0 Unported Licence.

24 D. D. Wang, L. Song, Y. Y. Wang, J. Y. Guo, H. Y. Shen, X. R. Wang and W. X. Chai, *Appl. Organomet. Chem.*, 2020, **34**, e5561.
25 M. Yoshida, S. Yanagida, D. Saito, A. Kobayashi and M. Kato, *Anal. Sci.*, 2020, **36**, 67.
26 T. H. Huang, Q. L. Hu, F. Z. Zhao, D. Zheng, Q. Liu, T. C. Wu, C. Luo, L. C. Gui and J. Chen, *J. Lumin.*, 2020, **227**, 117530.
27 L. Bergmann, J. Friedrichs, M. Mydlak, T. Baumann, M. Nieger and S. Bräse, *Chem. Commun.*, 2013, **49**, 6501.
28 H. Zhao, D. Jia, J. Li, G. J. Moxey and C. Zhang, *Inorg. Chim. Acta*, 2015, **432**, 1.
29 O. Stetsiuk, A. El-Ghayoury, A. Hauser and N. Avarvari, *Polyhedron*, 2019, **170**, 232.
30 J. Li and C. Zhang, *J. Chem. Sci.*, 2015, **127**, 1871.
31 J. Li, D. Jia, S. Meng, J. Zhang, M. P. Cifuentes, M. G. Humphrey and C. Zhang, *Chem. – Eur. J.*, 2015, **21**, 7914.
32 K. K. W. Lo, *Acc. Chem. Res.*, 2015, **48**, 2985.
33 A. Nayak, S. Patra, B. Sarkar, S. Ghumaan, V. G. Puranik, W. Kaim and G. K. Lahiri, *Polyhedron*, 2005, **24**, 333.
34 S. Ye, W. Kaim, B. Sarkar, B. Schwederski, F. Lissner, T. Schleid, C. Duboc-Toia and J. Fiedler, *Inorg. Chem. Commun.*, 2003, **6**, 1196.
35 M. Schwach, H. D. Hausen and W. Kaim, *Inorg. Chem.*, 1999, **38**, 2242.
36 M. Glöckle, K. Hübler, H. J. Kümmerer, G. Denninger and W. Kaim, *Inorg. Chem.*, 2001, **40**, 2263.
37 M. Maekawa, K. Sugimoto, T. Okubo, T. Kuroda-Sowa and M. Munakata, *Inorg. Chim. Acta*, 2017, **467**, 204.
38 W. Y. Yeh, G. H. Lee and S. M. Peng, *Inorg. Chim. Acta*, 2006, **359**, 659.
39 K. C. Gordon, A. K. Burrell, T. J. Simpson, S. E. Page, G. Kelso, M. I. J. Polson and A. Flood, *Eur. J. Inorg. Chem.*, 2002, **2002**, 554.
40 M. Alkan-Zambada, S. Keller, L. Martínez-Sarti, A. Prescimone, J. M. Junquera-Hernández, E. C. Constable, H. J. Bolink, M. Sessolo, E. Ortí and C. E. Housecroft, *J. Mater. Chem. C*, 2018, **6**, 8460.
41 C. Li, W. Li, A. F. Henwood, D. Hall, D. B. Cordes, A. M. Z. Slawin, V. Lemaur, Y. Olivier, I. D. W. Samuel and E. Zysman-Colman, *Inorg. Chem.*, 2020, **59**, 14772.
42 A. Jouaiti, L. Ballerini, H. L. Shen, R. Viel, F. Polo, N. Kyritsakas, S. Haacke, Y. T. Huang, C. W. Lu, C. Gourlaouen, H. C. Su and M. Mauro, *Angew. Chem., Int. Ed.*, 2023, **62**, e202305569.
43 Z. Liu, X. Wang, T. Lu, A. Yuan and X. Yan, *Carbon*, 2022, **187**, 78.
44 K. Suzuki, A. Kobayashi, S. Kaneko, K. Takehira, T. Yoshihara, H. Ishida, Y. Shiina, S. Oishi and S. Tobita, *Phys. Chem. Chem. Phys.*, 2009, **11**, 9850.
45 *Inorganic Electronic Structure and Spectroscopy*, ed. E. I. Solomon and A. B. P. Lever, Wiley, Hoboken, 2006, vol. I.
46 I. Andrés-Tomé, J. Fyson, F. B. Dias, A. P. Monkman, G. Iacobellis and P. Coppo, *Dalton Trans.*, 2012, **41**, 8669.
47 Y. Zhang, M. Heberle, M. Wächtler, K. Karnahl and B. Dietzek, *RSC Adv.*, 2016, **6**, 105801.
48 H. Bakkali, C. Marie, A. Ly, C. Thobie-Gautier, J. Graton, M. Pipelier, S. Sengmany, E. Léonel, J. Y. Nédélec, M. Evain and D. Dubreuil, *Eur. J. Org. Chem.*, 2008, 2156.
49 Y. Qu, F. X. Sauvage, G. Clavier, F. Miomandre and P. Audebert, *Angew. Chem., Int. Ed.*, 2018, **57**, 12057.
50 L. V. Hoff, S. D. Schnell, E. Benchimol, F. P. Foutinho, A. Tomio, M. Rickhaus and K. Gademann, *Helv. Chim. Acta*, 2023, **106**, e202200198.
51 I. S. Kritchenkov, J. R. Shakirova and S. P. Tunik, *RSC Adv.*, 2019, **9**, 15531.
52 Rigaku Oxford Diffraction, *CrysAlisPro 1.171.40.82a*, 2020.
53 G. M. Sheldrick, *Acta Crystallogr., Sect. A: Found. Adv.*, 2015, **71**, 3.
54 G. M. Sheldrick, *Acta Crystallogr., Sect. C: Struct. Chem.*, 2015, **71**, 3.
55 L. J. Bourhis, O. V. Dolomanov, R. Gildea, J. A. K. Howard and H. Puschmann, *Acta Crystallogr., Sect. A: Found. Adv.*, 2015, **71**, 59.
56 K. Brandenburg and H. Putz, *Diamond - Crystal and Molecular Structure Visualization Crystal Impact GbR, version 5.0.0*, Bonn, Germany.
57 P. van der Sluis and A. L. Spek, *Acta Crystallogr., Sect. A: Found. Crystallogr.*, 1990, **46**, 194.
58 F. Neese, *Comput. Mol. Sci.*, 2022, **12**, e1606.
59 (*a*) A. D. Becke, *Phys. Rev. A*, 1988, **38**, 3098; (*b*) J. P. Perdew, *Phys. Rev. B: Condens. Matter Mater. Phys.*, 1986, **33**, 8822.
60 E. Caldeweyher, S. Ehlert, A. Hansen, H. Neugebauer, S. Spicher, C. Bannwarth and S. Grimme, *J. Chem. Phys.*, 2019, **150**, 154122.
61 F. Weigend and R. Ahlrichs, *Phys. Chem. Chem. Phys.*, 2005, **7**, 3297.
62 F. Weigend, *Phys. Chem. Chem. Phys.*, 2006, **8**, 1057.
63 F. Neese, F. Wennmohs, A. Hansen and U. Becker, *Chem. Phys.*, 2009, **356**, 98.
64 M. Garcia-Ratés and F. Neese, *J. Comput. Chem.*, 2020, **41**, 922.
65 V. Barone and M. Cossi, *J. Phys. Chem. A*, 1998, **102**, 1995.
66 (*a*) C. Lee, W. Yang and R. G. Parr, *Phys. Rev. B: Condens. Matter*, 1988, **37**, 785; (*b*) A. D. Becke, *J. Chem. Phys.*, 1993, **98**, 1372; (*c*) A. D. Becke, *J. Chem. Phys.*, 1993, **98**, 5648; (*d*) P. J. Stephens, F. J. Devlin, C. F. Chabalowski and M. J. Frisch, *J. Phys. Chem.*, 1994, **98**, 11623.
67 K. Momma and F. Izumi, *J. Appl. Crystallogr.*, 2011, **44**, 1272.
68 (*a*) C. Müller, P. Wintergerst, S. S. Nair, N. Meitinger, S. Rau and B. Dietzek-Ivanšić, *J. Photochem. Photobiol., C*, 2022, **11**, 100130; (*b*) S. P. Y. Li, A. M. H. Yip, H. W. Lui and K. K. W. Lo, *Biomaterials*, 2016, **103**, 350; (*c*) A. M. H. Yip and K. K. W. Lo, *Coord. Chem. Rev.*, 2018, **361**, 138.

 This journal is © The Royal Society of Chemistry 2025